JOINT UNMIXING AND DEMOSAICING METHODS FOR SNAPSHOT SPECTRAL IMAGES

Kinan Abbas, Matthieu Puigt, Gilles Delmaire, and Gilles Roussel

Univ. Littoral Côte d'Opale, LISIC – UR 4491, F-62219 Longuenesse, France

ABSTRACT

Recent technological advances in design and processing speed have successfully demonstrated a new snapshot mosaic imaging sensor architecture (SSI), allowing miniaturized platforms to efficiently acquire the spatio-spectral content of the dynamic scenes from a single exposure. However, SSI systems have a fundamental trade-off between spatial and spectral resolution because they associate each pixel with a specific spectral band. In this paper, we introduce the problem of joint "demosaicing" and "unmixing" for the hyperspectral images acquired by the SSI camera that we formulate as a low-rank matrix factorization and completion problem. For that reason—and in addition to a "naive" approach—we extend the "pure pixel" framework to the SSI sensor patch level and propose a dedicated method which (i) assumes the observed data to be locally rank-1 in some SSI "patches" to find, (ii) estimates endmembers in these patches which are (iii) clustered to derive the actual spectra. The abundances are then recovered using nonnegative least squares in each patch. The experiments show that our proposed scheme provides a slightly better demosaicing performance than state-of-the-art methods and a much higher unmixing enhancement.

***Index Terms*—** Snapshot Spectral Imaging, Unmixing, Demosaicing, Low Rank Models,

1. INTRODUCTION

Recent Hyperspectral Imaging (HSI) architectures—known under the name of Spectral Snapshot Imaging (SSI)—have been proposed to allow HSI cameras to take images—or even videos—without requiring a repetitive scanning of the scene, which is classically met with standard HSI cameras [1]. To achieve this goal, SSI architectures associate each spatial pixel with a specific spectral band, thus introducing a critical trade-off between spatial and spectral resolution [2]. The SSI camera only acquires part of the HS data and then seeks to estimate the missing data in the post-processing method known as "demosaicing", for which many approaches have been proposed. Traditional methods use spatial and/or spectral correlation—and are based on Weighted Bilinear interpolation (WB) [3], Binary Tree-Based Generic Demosaicing (BTES) [4], Iterative Spectral Difference (ItSD) [5], a pseudo-panchromatic image (PPID) [6], structural and adaptive nonlocal optimization (SaND) [7], and graph-regularized low-rank matrix completion (GRMR) [2]—while deep learning methods were recently proposed [8–13].

On the other hand, hyperspectral unmixing is one of the essential techniques in analyzing hyperspectral images, which decomposes a mixed pixel into a collection of constituent materials weighted by their proportions. To do this, many algorithms for hyperspectral unmixing have been designed involving two steps: endmember extraction and mixed-pixel decomposition. The algorithms for identifying endmembers include, e.g., Pixel Purity Index (PPI), N-FINDR, or Vertex Component Analysis (VCA) [14]. Nonnegative matrix factorization (NMF) [15] is also a frequently used method in unmixing problems. It attempts to learn a part-based representation of the data, which is in accordance with how the brain recognizes objects. Lastly, Sparse Component Analysis (SCA) [16] is also a popular family of unmixing methods which has been applied to HSI unmixing in, e.g., [17, 18].

According to Tsagkatakis *et al.* [2], performing classification on SSI images after demosaicing provides a poor classification performance. For *in situ* mobile sensor calibration, it was found that coupling low-rank matrix completion and factorization was far more efficient than a two-stage approach consisting of a low-rank matrix completion followed by a matrix factorization [19]. In this work, we investigate if such behaviour also appears for SSI and we design a joint method for performing "demosaicing" and "unmixing" for the hyperspectral images acquired by the SSI camera. In particular, in addition to a naive approach straightforwardly derived from Weighted NMF (WNMF), we propose a novel approach which assumes that the abundances are sparse in a few sensor "patches" to find, so that a few of these patches to find are dominated by one unique endmember (as it is met with SCA, except that we consider partially observed data). Our proposed approach thus combines (i) rank-1 WNMF computed in "patches", (ii) a specific single-source confidence measure, (iii) a clustering stage to derive the endmembers, and (iv) a final estimation step of the abundances.

The remainder of the paper is organized as follows. We introduce the joint unmixing and demosaicing problem in Section 2. Section 3 introduces our proposed method whose performance is investigated in Section 4. We lastly conclude and introduce future work direction in Section 5.

2. PROBLEM STATEMENT

In this section, we define the SSI acquisition system and the problem we aim to solve. The considered SSI technology is based on a mosaic of Fabry-Perot filters [20, 21]. Each of these filters is passband and only allows the light from a very limited spectral range to propagate to a sensor cell. Conversely, it blocks the light outside this range. Consequently, in an *ideal* case[1], each pixel of the camera only captures one unique narrow band of wavelengths. The filters are organized in a mosaic pattern with the number of pixels equals to the number of wavelengths supported by the sensor. This mosaic pattern—aka sensor patch—is replicated over the active area of the sensor surface. Recovering the whole spectrum from such limited

K. Abbas greatly acknowledges the Région Hauts-de-France to partly fund his Ph.D. fellowship. Experiments presented in this paper were carried out using the CALCULCO computing platform, supported by SCoSI/ULCO.

[1] In the real case, the Fabry-Perot filters generate additional harmonics around each wavelength of interest. Taking into account these harmonics can be done within the framework of the methods proposed in this paper. However, due to space reasons, this is out of the scope of this paper.

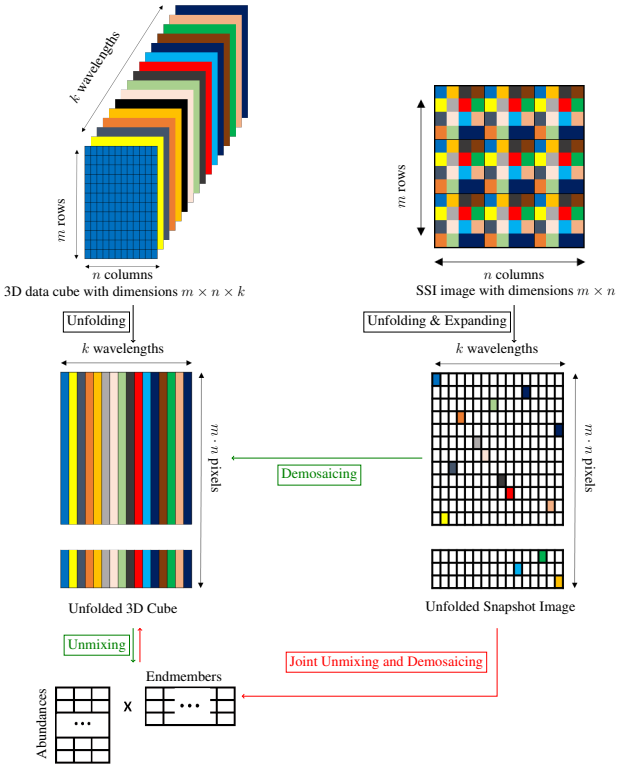

Fig. 1. Principles of the two-step (in green) and joint (in red) strategies.

information may be revisited as a low-rank matrix completion problem [2] (see Fig. 1).

Formally, an SSI camera acquires a two-dimensional image of $m \times n$ pixels, where m and n are the numbers of pixels in the horizontal and vertical dimensions, respectively. Each spatial pixel out of the $m{\cdot}n$ available ones is associated with a different spectral band out of k bands which are supposed to be acquired by the camera. More specifically, this implies that an SSI image is a 2D projection of a 3D $m \times n \times k$ theoretical datacube that we now model.

Following an unfolding strategy classically used in unmixing, we rewrite the theoretical 3D datacube as an $(m \cdot n) \times k$ matrix, i.e., a matrix Y whose row indices correspond to a spatial position while column indices are linked to wavelengths. As proposed in [2], it is then possible to derive an $(m \cdot n) \times k$ data matrix with missing entries denoted X. Both matrices X and Y are linked through

$$W \circ X = W \circ Y, \tag{1}$$

where W denotes a binary weight matrix whose nonzero entries allow to select which wavelength is observed by the camera, and $\circ$ denotes the Hadamard product. Similarly, unfolding the $m \times n$ SSI image as we did for the data cube Y leads to an $(m \cdot n) \times 1$ vector $\underline{z}$ whose i-th entry is the non-null value of the i-th row of X. As W is known, deriving X from $\underline{z}$ is straightforward and vice-versa. We can thus assume that X is the original data matrix we get from the SSI acquisition process. Recovering Y from X corresponds to "demosaicing" the SSI image. In practice, it may be solved by, e.g., additionally assuming that Y is low-rank [2].

We further assume that each row of Y may be expressed as a linear mixture of the spectra of the materials observed by the camera—a.k.a. endmembers—i.e.,

$$Y \approx G \cdot F, \tag{2}$$

where F denotes the $p \times k$ matrix of endmembers, G denotes the $(m \cdot n) \times p$ abundance matrix, and p is the number of endmembers which are present in the scene. Equation (2) is not only a very classical model met in hyperspectral unmixing [14] but also a low-rank approximation model, provided $p < \min\{(m \cdot n), k\}$. Combining Eqs. (1) and (2) provides the considered joint "demosaicing" and "unmixing" model, i.e.,

$$W \circ X \approx W \circ (G \cdot F). \tag{3}$$

Indeed, if one may completely estimate G and F from the partially observed matrix X, the product $G \cdot F$ is an estimation of Y and—following a classical matrix completion framework—one may derive

$$\hat{Y} = W \circ X + (\mathbb{1}_{(m \cdot n) \times k} - W) \circ (G \cdot F), \tag{4}$$

where $\mathbb{1}_{(m \cdot n) \times k}$ denotes the $(m{\cdot}n) \times k$ matrix of ones. Furthermore, the content of G and F may be useful for several applications, e.g., for spectral library learning—using F—or for land use / cover which are derived from G. Let us stress again that we aim to compare the performance between a 2-stage strategy—consisting of a demosaicing step where Y is estimated followed by an unmixing one where G and F are derived, i.e., the green framework in Fig. 1—and a joint demosaicing and unmixing strategy shown in red in Fig. 1, for which we propose a dedicated method in Section 3.

3. PROPOSED METHODS

We now introduce our proposed methods. We actually propose two joint demosaicing and unmixing methods. More specifically, we first introduce a "naive" approach which is derived from weighted NMF, following the strategy in [19] for another application. We then propose a novel method specifically designed for SSI data.

3.1. Naive Method

We first introduce a naive method that is derived from Section 2. Such a method should solve Eq. (3) which is an instance of Weighted NMF (WNMF). WNMF can be solved using several strategies, i.e., (i) adding the weights in the update rules [22], (ii) considering an Expectation-Maximization (EM) Framework [23], or (iii) applying a stochastic gradient descent by selecting only the available data. The second strategy was found in [23] to be much faster and more accurate than the first one—especially when combined with a Nesterov solver (NeNMF [24])—and more versatile than stochastic methods only able to perform binary weights. Such a method is chosen as a baseline for comparison with a dedicated method proposed hereafter.

3.2. Clustering and Rank-1-based Proposed Technique

We here introduce our proposed method. It finds its roots in the most basic way to restore the datacube. Indeed, the image sensor is divided as patches which are repeated over the sensor surface. Each patch is of size $\sqrt{k} \times \sqrt{k}$ (typically, $k = 16$ or 25, so that a patch is of size 4×4 or 5×5). One may then assume that each patch corresponds to a "super-pixel", i.e., that each patch is linked with a unique endmember. In practice, such an assumption is wrong, hence the fact that many demosaicing methods have been proposed. However, this assumption may be valid for a few patches to find, where

one endmember is dominant over the others. This may be related to the pure-pixel assumption [14] or abundance sparsity in SCA [16]. However, the main difference between our considered problem and the one met with classical unmixing relies on the fact that we only partially observe the datacube over a patch, and we aim to infer it from a few available samples. This allows us to state our first assumption.

Assumption 1 (Pure patch assumption) *For each endmember, there exists at least one sensor patch where only this endmember is present.*

Our proposed method reads as follows. We denote by X_i, Y_i, and W_i the $k \times k$ sub-matrices of X, Y and W, respectively, corresponding to Patch i. We derive a rank-1 approximation of Y_i from X_i using the above WNMF strategy, i.e.,

$$W_i \circ X_i \approx W_i \circ (\underline{g}_i \cdot \mathbf{f}_i), \tag{5}$$

where $\underline{g}_i$ denotes a column vector and $\mathbf{f}_i$ denotes a row vector.

Algorithm 1 K-means (resp. K-medians) Patch-based Weighted Non-negative Matrix Factorization (KPWNMF)

Input:
X is the unfolded SSI image of rank p weighted by W
Output:
$\hat{Y}^{\text{final}}$ the restored unfolded data cube
$[G, F]$ final abundances and endmembers matrices
Processing:

for $i = 1$ **to** nb_patches **do**
  Let the submatrices X_i and W_i linked to Patch i
  Initialize $\underline{g}_i$ and $\mathbf{f}_i$
  for $\text{Counter}_1 = 1$ **to** $\text{Max}_{\text{outerIter}}$ **do**
    $X_i^{\text{Comp}} = W_i \circ X_i + (\mathbb{1}_{k\times k} - W_i) \circ (\underline{g}_i \times \mathbf{f}_i)$
    for $\text{Counter}_2 = 1$ **to** $\text{Max}_{\text{innerIter}}$ **do**
      Update $\underline{g}_i$ from X_i^{Comp} and $\mathbf{f}_i$ using NeNMF
      Update $\mathbf{f}_i$ from X_i^{Comp} and $\underline{g}_i$ using NeNMF
  Append $\mathbf{f}_i$ to the pool F^{pool}
$F = \text{k-means}(F^{pool}, p)$ (resp. $F = \text{k-medians}(F^{pool}, p)$)
Derive X^{comp} from the last estimates of X_i^{Comp} in each patch
Initialize G of size $(m \cdot n) \times p$
Update G from X^{Comp} and F using NeNMF
Compute $\hat{Y}^{\text{final}}$ using Eq. (4)

If only one endmember is present in the patch—i.e., if Assumption 1 is satisfied—then the considered patch is rank-1, and the rank-1 approximation from partial data in X_i allows to estimate the endmember $\mathbf{f}_i$. However, if several endmembers are present in the patch, we must not detect the patch as pure. This brings a second assumption.

Assumption 2 *In the patches where several endmembers are present, their abundances significantly vary over each patch.*

Assumption 2 is classically stated in SCA [16]. In practical scenarios, the SSI camera should be close-enough to the scene that it is observing, so that one may not expect multiple abundances to remain in constant proportions over a patch. As a consequence, if the considered i-th patch is approximately pure, then

$$\|W_i \circ X_i - W_i \circ (\underline{g}_i \cdot \mathbf{f}_i)\|_F^2 \approx 0. \tag{6}$$

On the contrary, if this patch is not pure, then

$$\|W_i \circ X_i - W_i \circ (\underline{g}_i \cdot \mathbf{f}_i)\|_F^2 \gg 0. \tag{7}$$

Such an error can thus be seen as a "single-source confidence measure" as those classically used in SCA. We thus derive from each patch one noisy estimation of one "true" endmember. These estimates are further assumed to be arranged as clusters of spectra distributed around the "true" source spectra. We thus can use any clustering method—e.g., K-means or K-medians—to derive the actual endmembers. A refined strategy consists of selecting the patches where the above squared Frobenius norm is small-enough[2]. This yields to a reduced set of spectra which are each closer to the "true" ones. Such a strategy is similar to the *Selective* K-means or K-medians methods proposed in [25] and was found to significantly improve the unmixing and demosaicing performance of our proposed approach in preliminary tests. We thus choose these methods in this paper. Once the actual endmembers are derived and stored in the matrix F, the abundance matrix G is re-estimated using NeNMF [24] with the fixed matrix F, i.e., as a nonnegative least-square problem. The whole strategy is provided in Algorithm 1.

4. EXPERIMENTS AND RESULTS

To assess the performance of the proposed method, we conduct experiments on SSI simulations derived from synthetic images and the CAVE dataset [26]. The former allows for the measurement of the unmixing and demosaicing performance, while the latter is used to measure the demosaicing performance. For the synthetic experiment, we create one "simple" image and one "more complex" one. Each one has 100×100 pixels with three endmembers, i.e., water, metal, and concrete whose signatures are taken from [27]. Both images simulate a scene observed from a short distance which implies that many patches are pure. However, the complex image does not satisfy Assumption 2. We thus expect the performance of the proposed method to be significantly degraded with this image. We consider 4×4 and 5×5 spectral filter patterns, Lastly, we test the performance under different noise levels. For the CAVE dataset, we use all the images in the dataset, and we simulate the 4×4 and 5×5 SSI images using the same strategy as in [2].

We compare the performance reached with the naive WNMF method with our proposed approach—denoted KPWNMF for K-means[3] Patch-based WNMF—and five 2-step demosaicing-then-unmixing methods. For the latter, we consider five SotA demosaicing methods—i.e., GMRM [2], BTES [4], WB [3], PPID [6], and ItSD [5]—while in the second step we unmix the restored datacube Y using NeNMF [24].

To measure the performance of the tested methods, we investigate their demosaicing enhancement—which consists of comparing the estimated Y matrices to the true ones—that we measure using the Peak Signal-to-Noise Ratio (PSNR), while the unmixing enhancement is observed using the Signal-to-Interference Ratio (SIR) and the Spectral Angle Mapper (SAM) for endmember estimation and the Mixing Error Ratio (MER) for measuring the quality of the abundance maps. Fig. 2 shows the demosaicing performance—depicted by the PSNR values in dB—and the unmixing performance—depicted by the SAM and SIR values for the

[2]Estimating the threshold to decide weither a patch is pure or not is out of the scope of this paper. In the experiments provided in Sect. 4, it is set as the median of all the patch norm errors.

[3]We found K-means and K-medians to provide the same clustering performance in these tests, and we do not show the former for space considerations.

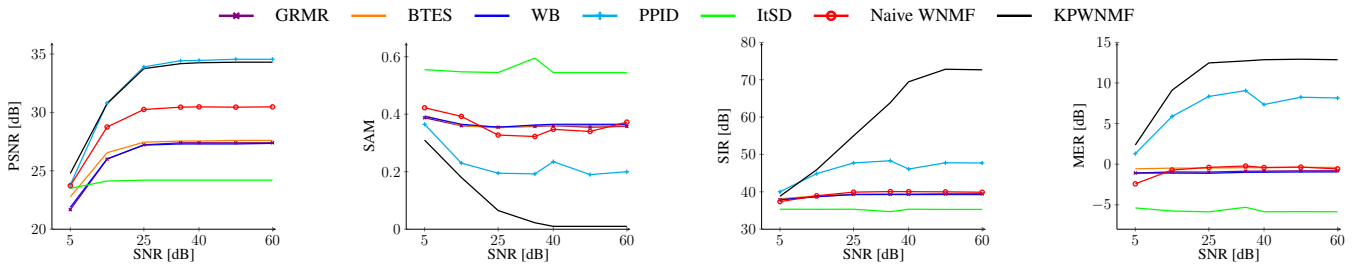

Fig. 2. From left to right: mean PSNR, SAM, SIR and MER—obtained for both images with 4×4 and 5×5 filters—relative to input SNR.

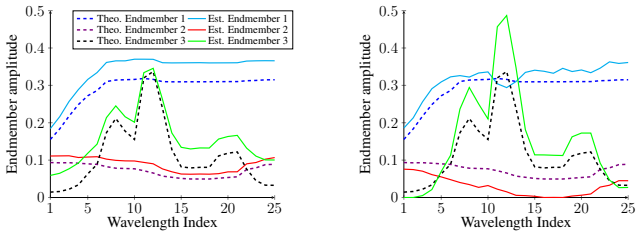

(a) KPWNMF (b) PPID + Unmixing

Fig. 3. Estimated spectra in case of the synthetic image where Assumption 2 is violated, with Fabry-Perot filter of size 5×5.

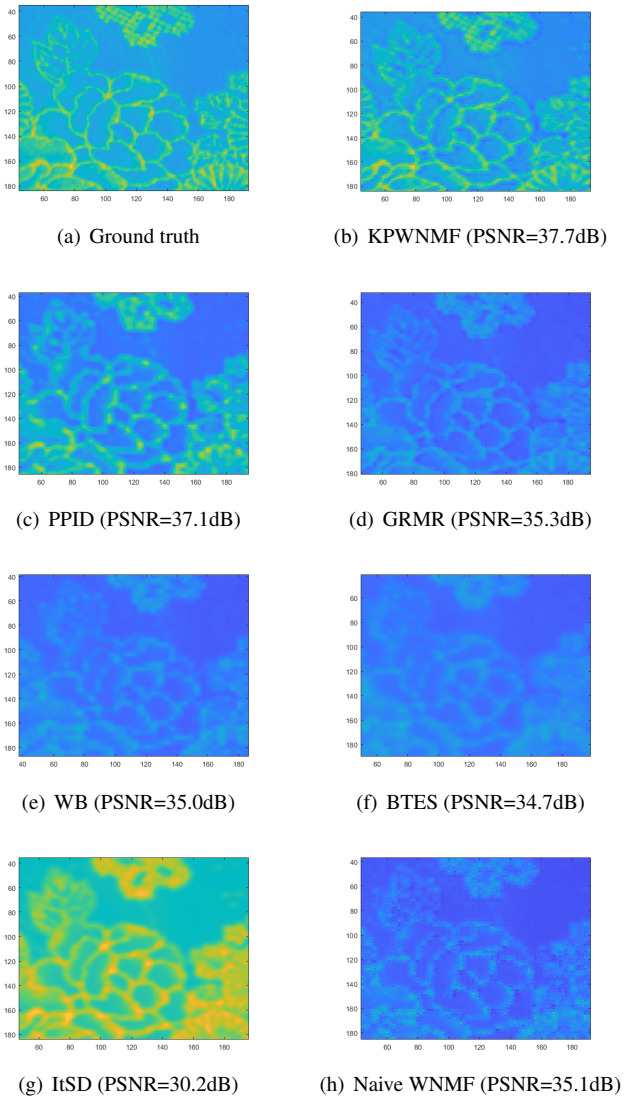

(a) Ground truth (b) KPWNMF (PSNR=37.7dB)
(c) PPID (PSNR=37.1dB) (d) GRMR (PSNR=35.3dB)
(e) WB (PSNR=35.0dB) (f) BTES (PSNR=34.7dB)
(g) ItSD (PSNR=30.2dB) (h) Naive WNMF (PSNR=35.1dB)

Fig. 4. Demosaiced images obtained with KPWNMF and SotA methods for the 4×4 patch, and PSNRs averaged over all the images.

endmember estimation and by the MER values for the abundance estimation—with respect to some input SNR. This figure shows the proposed method to significantly outperform the other tested methods in unmixing while providing a similar demosaicing than PPID, i.e., the best SotA demosaicing method in these tests.

Fig. 3 shows the true and estimated endmembers with the complex synthetic image and the 5×5 patch. Let us recall that this image satisfies Assumption 1 but not Assumption 2. As a consequence, the reached performance with KPWNMF is lower than with the simple image. Still, it provides better estimates than the 2-stage approach using PPID which does not require any of these assumptions.

In order to validate the demosaicing merits of the proposed approach, we provide comparative results with the SoTA methods on the CAVE dataset. Fig. 4 shows the "Cloth" image at one band after demosaicing with the average PSNR of every method computed over all the images in the CAVE dataset. As we can see from the figure, the proposed approach surpasses all the SoTA approaches in average PSNR and in the ability to restore the tiny details of the shapes, which shows the relevance of our work.

5. CONCLUSION AND DISCUSSION

In this paper, we proposed a novel joint unmixing and demosaicing method for SSI images. It combines a patch-based rank-1 assumption with a dedicated single-source confidence measure to estimate the endmembers whose actual estimates are obtained using clustering. The abundances are then re-estimated using nonnegative least-squares. In realistic simulations of SSI data, we found that our proposed approach not only outperforms the unmixing performance of two-step approaches—consisting of a demosaicing stage followed by an unmixing one—but also provides a better or similar demosaicing performance. It also outperforms a naive WNMF approach that is straightforwardly derived from the problem statement. In future work, we aim to investigate the use of our proposed method on real SSI data. We also aim to extend it to the case when endmember spectral variability is met in the acquisition process [28].

6. REFERENCES

[1] D. Manolakis, R. Lockwood, and T. Cooley, *Hyperspectral Imaging Remote Sensing*, Cambridge University Press, 2016.

[2] G. Tsagkatakis, M. Bloemen, B. Geelen, M. Jayapala, and P. Tsakalides, "Graph and rank regularized matrix recovery for snapshot spectral image demosaicing," *IEEE Trans. Comput. Imaging*, vol. 5, no. 2, pp. 301–316, June 2019.

[3] J. Brauers and T. Aach, "A color filter array based multispectral camera," in *12. Workshop Farbbildverarbeitung*, G. C. Group, Ed., Ilmenau, October 5-6 2006.

[4] L. Miao, H. Qi, R. Ramanath, and W. Snyder, "Binary tree-based generic demosaicking algorithm for multispectral filter arrays," *IEEE Trans. Image Process.*, vol. 15, no. 11, pp. 3550–3558, Nov. 2006.

[5] J. Mizutani, S. S. Ogawa, K. Shinoda, M. Hasegawa, and S. Kato, "Multispectral demosaicking algorithm based on inter-channel correlation," in *Proc. IEEE VCIP'14*, 2014, pp. 474–477.

[6] S. Mihoubi, O. Losson, B. Mathon, and L. Macaire, "Multispectral demosaicing using pseudo-panchromatic image," *IEEE Trans. Comput. Imaging*, vol. 3, no. 4, pp. 982–995, Dec. 2017.

[7] L. Bian, Y. Wang, and J. Zhang, "Generalized MSFA engineering with structural and adaptive nonlocal demosaicing," *IEEE Trans. Image Process.*, vol. 30, pp. 7867–7877, 2021.

[8] K. Dijkstra, J. van de Loosdrecht, L. R. B. Schomaker, and M. A. Wiering, "Hyperspectral demosaicking and crosstalk correction using deep learning," *Machine Vision and Applications*, vol. 30, no. 1, pp. 1–21, July 2018.

[9] T. A. Habtegebrial, G. Reis, and D. Stricker, "Deep convolutional networks for snapshot hypercpectral demosaicking," in *Proc. IEEE WHISPERS'19*, Sept. 2019.

[10] Z. Pan, B. Li, H. Cheng, and Y. Bao, "Joint demosaicking and denoising for CFA and MSFA images using a mosaic-adaptive dense residual network," in *Computer Vision – ECCV 2020 Workshops*, pp. 647–664. Springer International Publishing, 2020.

[11] K. Feng, Y. Zhao, J. C.-W. Chan, S. Kong, X. Zhang, and B. Wang, "Mosaic convolution-attention network for demosaicing multispectral filter array images," *IEEE Trans. Comput. Imaging*, vol. 7, pp. 864–878, 2021.

[12] T. Zhang, Z. Liang, and Y. Fu, "Joint spatial-spectral pattern optimization and hyperspectral image reconstruction," *IEEE J. Sel. Topics Signal Process.*, vol. 16, no. 4, pp. 636–648, 2022.

[13] P. Li, M. Ebner, P. Noonan, C. Horgan, A. Bahl, S. Ourselin, J. Shapey, and T. Vercauteren, "Deep learning approach for hyperspectral image demosaicking, spectral correction and high-resolution RGB reconstruction," *Computer Methods in Biomechanics and Biomedical Engineering: Imaging & Visualization*, vol. 10, no. 4, pp. 409–417, 2022.

[14] J. M. Bioucas-Dias, A. Plaza, N. Dobigeon, M. Parente, Q. Du, P. Gader, and J. Chanussot, "Hyperspectral unmixing overview: Geometrical, statistical, and sparse regression-based approaches," *IEEE J. Sel. Topics Appl. Earth Observ. Remote Sens.*, vol. 5, no. 2, pp. 354–379, Apr. 2012.

[15] D. D. Lee and H. S. Seung, "Learning the parts of objects by non-negative matrix factorization," *Nature*, vol. 401, no. 6755, pp. 788–791, Oct. 1999.

[16] Y. Deville, "Sparse component analysis: A general framework for linear and nonlinear blind source separation and mixture identification," in *Blind Source Separation*, pp. 151–196. Springer, 2014.

[17] O. Berné, C. Joblin, A. Tielens, Y. Deville, M. Puigt, R. Guidara, S. Hosseini, G. Mulas, and J. Cami, "Source separation algorithms for the analysis of hyperspectral observations of very small interstellar dust particles," in *Proc. IEEE WHISPERS'09*, 2009, pp. 1–4.

[18] M. S. Karoui, Y. Deville, S. Hosseini, and A. Ouamri, "Blind spatial unmixing of multispectral images: New methods combining sparse component analysis, clustering and non-negativity constraints," *Pattern Recognition*, vol. 45, no. 12, pp. 4263–4278, 2012.

[19] C. Dorffer, M. Puigt, G. Delmaire, and G. Roussel, "Informed nonnegative matrix factorization methods for mobile sensor network calibration," *IEEE Trans. Signal Inf. Process. Netw.*, vol. 4, no. 4, pp. 667–682, 2018.

[20] B. Geelen, N. Tack, and A. Lambrechts, "A compact snapshot multispectral imager with a monolithically integrated per-pixel filter mosaic," in *Advanced Fabrication Technologies for Micro/Nano Optics and Photonics VII*, G. von Freymann, W. V. Schoenfeld, and R. C. Rumpf, Eds. Mar. 2014, SPIE.

[21] B. Geelen, C. Blanch, P. Gonzalez, N. Tack, and A. Lambrechts, "A tiny VIS-NIR snapshot multispectral camera," in *Advanced Fabrication Technologies for Micro/Nano Optics and Photonics VIII*, G. von Freymann, W. V. Schoenfeld, R. C. Rumpf, and H. Helvajian, Eds. Mar. 2015, SPIE.

[22] N.-D. Ho, *Non negative matrix factorization algorithms and applications*, Phd thesis, Université Catholique de Louvain, 2008.

[23] C. Dorffer, M. Puigt, G. Delmaire, and G. Roussel, "Fast nonnegative matrix factorization and completion using Nesterov iterations," in *Proc. LVA/ICA'17*, Feb. 2017, vol. 10169 of *LNCS*, pp. 26–35.

[24] N. Guan, D. Tao, Z. Luo, and B. Yuan, "NeNMF: An optimal gradient method for nonnegative matrix factorization," *IEEE Trans. Signal Process.*, vol. 60, no. 6, pp. 2882–2898, June 2012.

[25] M. Puigt and Y. Deville, "Iterative-shift cluster-based time-frequency BSS for fractional-time-delay mixtures," in *Proc. ICA'09*, 2009, pp. 306–313.

[26] F. Yasuma, T. Mitsunaga, D. Iso, and S. Nayar, "Generalized Assorted Pixel Camera: Post-Capture Control of Resolution, Dynamic Range and Spectrum," Tech. Rep., Nov 2008.

[27] "U.S. Geological Survey (USGS) spectral library," `https://www.usgs.gov/labs/spectroscopy-lab/science/spectral-library`, Last accessed: 2022-10-24.

[28] R. A. Borsoi, T. Imbiriba, J. C. M. Bermudez, C. Richard, J. Chanussot, L. Drumetz, J.-Y. Tourneret, A. Zare, and C. Jutten, "Spectral variability in hyperspectral data unmixing: A comprehensive review," *IEEE Trans. Geosci. Remote Sens.*, vol. 9, no. 4, pp. 223–270, 2021.